A FLUID TRANSIENT ANALYSIS FOR THE PROPELLANT FLOW IN A MONOPROPELLANT PROPULSION SYSTEM

Jongwon Chae[1]

단일추진체 추진시스템의 과도기유체 해석

채 종 원

A fluid transient analysis for the propellant flow in a monopropellant propulsion system is conducted by using the method of characteristics(MOC). It reviews algebraic simultaneous equations method and Cramer's rule method utilized to drive the compatible and characteristic equations to understand MOC extensively. The identification of fluid transient phenomena of propulsion system of Koreasat 1 is carried out through parametric studies. The valve response time is one of the dominant parameters governing the fluid transient phenomena. The results show that the shorter closing time induces the greater pressure response amplitude. And it shows that the installation of in-line orifice is effectively to limit the fluid transients in rapid valve response time and at high pressure. But it seems that the effect of orifice weakens at slow valve response time and at low pressures.

Key Words: Transient Flow, Method of Characteristics, Propellant

1. INTRODUCTION

Fluid transient analysis essentially consists of solving the governing equations for a wide variety of boundary and initial conditions, and system topologies. Since the equations cannot be analytically solved, many methods have been developed over the years. The method of characteristics is usually adopted for transient phenomena analysis. Its strong point is to transform the two partial differential equations(PDEs) of continuity and momentum conservations into four ordinary differential equations(ODEs) that are solved numerically using finite difference techniques[1,2,3].

A fluid transient analysis for the propellant flow in a satellite propulsion system is needed to verify the design of propulsion system. This work is not to verify the design of propulsion system of Koreasat 1 but to identify it through parametric studies. Main parameter is the thruster valve operation time, and given conditions are pipeline materials and number of pressure drop devices(i.e. filters, latching isolation valves, etc.) and pipelines, their lengths and topologies. They are fully considered in a model to analyze fluid transients.

Received: March 30, 2005, Accepted: May 1, 2005.
1 정회원, 한국항공우주연구원 체계종합그룹(통신해양)
E-mail: firstbel@kari.re.kr

2. DERIVATIONS

2.1 BASIC DIFFERENTIAL EQUATIONS FOR TRANSIENT FLOW

The one-dimensional unsteady pressure flow equations are given by

$$gH_x + V_t + \frac{f}{2D}V|V| = 0 \tag{1}$$

$$H_t + \frac{a^2}{g}V_x = 0 \tag{2}$$

where f is the Darcy-Weisbach friction coefficient. The momentum equation (1) and continuity equation (2) form a pair of quasi-linear hyperbolic partial differential equations in terms of two dependent variables, velocity(V) and hydraulic-grad-line elevation(H), and two independent variables, distance along the pipe(x) and time(t). The equations are transformed into four ordinary differential equations by using the method of characteristics. The subscripts x and t denote partial differentiation(i.e., $H_x = \partial H/\partial x$). In the following section the derivation of four ordinary differential equations are reviewed and based on[1] and[4] in order to understand the method of characteristics extensively.

2.2 ALGEBRAIC SIMULTANEOUS EQUATIONS AND CALCULUS

The simplified equations of motion and continuity are identified as L_1 and L_2 [from Eqs. (1) and (2)]:

$$L_1 = gH_x + V_t + \frac{f}{2D}V|V| = 0 \tag{3}$$

$$L_2 = H_t + \frac{a^2}{g}V_x = 0 \tag{4}$$

These equations are combined linearly using an unknown multiplier λ:

$$\begin{aligned} L &= L_1 + \lambda L_2 \\ &= gH_x + V_t + \frac{f}{2D}V|V| + \lambda\left(H_t + \frac{a^2}{g}V_x\right) \\ &= \lambda\left(H_x\frac{g}{\lambda} + H_t\right) + \left(V_x\lambda\frac{a^2}{g} + V_t\right) + \frac{f}{2D}V|V| \\ &= 0 \end{aligned} \tag{5}$$

Any two real, distinct values of λ will again yield two equations in terms of the two dependent variables H and V that are in every way the equivalent of Eqs. (1) and (2). Appropriate selection of two particular values of λ leads to simplification of Eq. (5). In general, both variables H and V are functions of x and t. If the independent variable x is permitted to be a function of t, then, from total differential of calculus,

$$\frac{dH}{dt} = H_x\frac{dx}{dt} + H_t, \quad \frac{dV}{dt} = V_x\frac{dx}{dt} + V_t \tag{6}$$

Now, by examination of Eq. (5) with Eqs. (6) in mind, it can be noted that if

$$\frac{dx}{dt} = \frac{g}{\lambda} = \frac{\lambda a^2}{g} \tag{7}$$

Eq. (5) becomes the ordinary differential equation

$$\lambda\frac{dH}{dt} + \frac{dV}{dt} + \frac{f}{2D}V|V| = 0 \tag{8}$$

The solution of Eq. (7) yields the two particular values of λ,

$$\lambda = \pm\frac{g}{a} \tag{9}$$

By substituting these values of λ back into Eq. (7), the particular manner in which x and t are related is given:

$$\frac{dx}{dt} = \pm a \tag{10}$$

This shows the change in position of a wave related to the change in time by the wave propagation velocity a. When the positive value of λ is used in Eq. (7), the positive value of λ must be used in Eq. (8). A similar parallelism exists for the negative λ. The substitution of these values of λ into Eq. (8) leads to two pairs of equations which are grouped and identified as C+ and C- equations.

$$C^+ : \begin{cases} \dfrac{g}{a}\dfrac{dH}{dt} + \dfrac{dV}{dt} + \dfrac{f}{2D}V|V| = 0 & (11) \\ \dfrac{dx}{dt} = +a & (12) \end{cases}$$

$$C^- : \begin{cases} -\dfrac{g}{a}\dfrac{dH}{dt} + \dfrac{dV}{dt} + \dfrac{f}{2D}V|V| = 0 & (13) \\ \dfrac{dx}{dt} = -a & (14) \end{cases}$$

Thus two real values of λ have been used to convert the original two partial differential equations to

two total (ordinary) differential equations, Eqs. (11) and (13), each with the restriction that it is valid only when the respective Eqs. (12) and (14) are valid.

It is convenient to visualize the solution as it develops on the independent variable plane (i.e., the xt plane). Inasmuch as a is generally constant for a given pipe, Eq. (12) plots as a straight line on the xt plane; and similarly, Eq. (14) plots as a different straight line as shown in Fig. 1. These lines on the xt plane are the "characteristic" lines along which Eqs. (11) and (13) are valid. The latter equations are referred to as compatibility equations, each one being valid only on the appropriate characteristic line. No mathematical approximations have been made in this transformation of the original partial differential equations. Thus every solution of this set will be a solution of the original system given by Eqs. (3) and (4).

2.3 A METHOD BASED ON CRAMER'S RULE

Rearrange the system of quasi-linear equations given Eqs. (1), (2) and (6) as

$$gH_x + V_t = -\frac{f}{2D}V|V| \tag{15}$$

$$H_t + \frac{a^2}{g}V_x = 0 \tag{16}$$

$$dH = H_x dx + H_t dt \tag{17}$$

$$dV = V_x dx + V_t dt \tag{18}$$

Eqs. (15) through (18) constitute a system of four linear equations with four unknowns (H_x, H_t, V_x, and V_t). These equations can be written in matrix form as

$$\begin{bmatrix} g & 0 & 0 & 1 \\ 0 & 1 & \frac{a^2}{g} & 0 \\ dx & dt & 0 & 0 \\ 0 & 0 & dx & dt \end{bmatrix} \begin{bmatrix} H_x \\ H_t \\ V_x \\ V_t \end{bmatrix} = \begin{bmatrix} -\frac{f}{2D}V|V| \\ 0 \\ dH \\ dV \end{bmatrix} \tag{19}$$

Let [A] denote the coefficient matrix.

$$[A] = \begin{bmatrix} g & 0 & 0 & 1 \\ 0 & 1 & \frac{a^2}{g} & 0 \\ dx & dt & 0 & 0 \\ 0 & 0 & dx & dt \end{bmatrix} \tag{20}$$

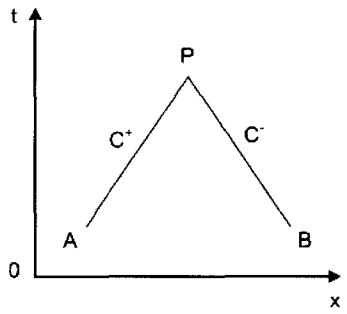

Fig. 1 Characteristic lines in the xt plane

Let us solve Eq. (19) for the unknown Hx, using Cramer's rule. To do this, we define the matrix [B] as the matrix [A] with its first column replaced by the column vector on the right-hand side of Eq. (19), i.e.,

$$[B] = \begin{bmatrix} -\frac{f}{2D}V|V| & 0 & 0 & 1 \\ 0 & 1 & \frac{a^2}{g} & 0 \\ dH & dt & 0 & 0 \\ dV & 0 & dx & dt \end{bmatrix} \tag{21}$$

Denoting the determinants of [A] and [B] by |A| and |B|, respectively, Cramer's rule gives the solution for Hx as

$$H_x = \frac{|B|}{|A|} \tag{22}$$

Recall from linear algebra that, if a square coefficient matrix for a set of n linear equations has a vanishing determinant, then a necessary condition for finite solutions to exist is that when the RHS is substituted for any column of the coefficient matrix, the resulting determinant must also vanish(cf., the Cramer's rule for solving linear systems of equations).

If only |A| were zero, then H_x would be infinite. However, the definition of a characteristic line states that H_x be indeterminant along the characteristic, not infinite. Thus, for H_x to be indeterminant, |B| in Eq. (22) must also be zero. Then, H_x is of the form

$$H_x = \frac{|B|}{|A|} = \frac{0}{0} \tag{23}$$

namely, an indeterminant form which can have a finite value. Hence, from Eqs. (20) and (21)

$$|A| = \begin{vmatrix} g & 0 & 0 & 1 \\ 0 & 1 & \frac{a^2}{g} & 0 \\ dx & dt & 0 & 0 \\ 0 & 0 & dx & dt \end{vmatrix} = 0 \tag{24}$$

$$|B| = \begin{vmatrix} -\frac{f}{2D}V|V| & 0 & 0 & 1 \\ 0 & 1 & \frac{a^2}{g} & 0 \\ dH & dt & 0 & 0 \\ dV & 0 & dx & dt \end{vmatrix} = 0 \tag{25}$$

Expansion of the determinant in Eq. (24) yields a characteristic line as Eq. (10). Expansion of the determinant in Eq. (25) yields an ordinary differential equation in term of dH and dV, where dx and dt are restricted to hold along a characteristic line. The equation for the dependent variables H and V which comes from Eq. (25) is called the compatibility equation as Eqs (11) and (13). It is an equation involving the unknown dependent variables which holds only along the characteristic line; the advantage of this compatibility equation is that it is in one less dimension than the original partial differential equations. Since the governing equations given in this paper are partial differential equations in two dimensions, then the compatibility equation is in one dimension-hence it is an ordinary differential equation-and the "one dimension" is along the characteristic direction.

2.4 A METHOD BASED ON EIGENVALUES OF THE SYSTEM

The eigenvalue method is based on a display of the system of partial differential equations, Eqs. (1) and (2) written in column vector form.

Defining W as the column vector

$$W = \begin{bmatrix} H \\ V \end{bmatrix} \tag{26}$$

the system of equation given by Eqs. (1) and (2) can be written as

$$\begin{bmatrix} g & 0 \\ 0 & \frac{a^2}{g} \end{bmatrix} \frac{\partial W}{\partial x} + \begin{bmatrix} 0 & 1 \\ 1 & 0 \end{bmatrix} \frac{\partial W}{\partial t} = \begin{bmatrix} -\frac{f}{2D}V|V| \\ 0 \end{bmatrix} \tag{27}$$

or

$$[K]\frac{\partial W}{\partial x} + [M]\frac{\partial W}{\partial t} = \begin{bmatrix} -\frac{f}{2D}V|V| \\ 0 \end{bmatrix} \tag{28}$$

where [K] and [M] are the appropriate 2 x 2 matrices in Eq. (27). Multiplying Eq. (27) by the inverse of [K], we have

$$\frac{\partial W}{\partial x} + [K]^{-1}[M]\frac{\partial W}{\partial t} = [K]^{-1}\begin{bmatrix} -\frac{f}{2D}V|V| \\ 0 \end{bmatrix} \tag{29}$$

or

$$\frac{\partial W}{\partial x} + [N]\frac{\partial W}{\partial t} = [K]^{-1}\begin{bmatrix} -\frac{f}{2D}V|V| \\ 0 \end{bmatrix} \tag{30}$$

where by definition $[N]=[K]^{-1}[M]$. The eigenvalues of [N] are precisely the slopes of the characteristic lines and determine the classification of the system. If the eigenvalues are all real, the equations are hyperbolic. If the eigenvalues are all complex, the equations are elliptic.

The eigenvalues of [N] is examined as

$$[N] = [K]^{-1}[M] = \begin{bmatrix} g & 0 \\ 0 & \frac{a^2}{g} \end{bmatrix}^{-1}\begin{bmatrix} 0 & 1 \\ 1 & 0 \end{bmatrix} = \begin{bmatrix} 0 & \frac{1}{g} \\ \frac{g}{a^2} & 0 \end{bmatrix} \tag{31}$$

$$|[N] - \lambda[I]| = 0 \tag{32}$$

where [I] is the identity matrix. Hence

$$\begin{vmatrix} -\lambda & \frac{1}{g} \\ \frac{g}{a^2} & -\lambda \end{vmatrix} = 0 \tag{33}$$

Expanding the determinant, we have

$$\lambda^2 - \frac{1}{a^2} = 0 \tag{34}$$

or

$$\lambda = \pm\frac{1}{a} = \frac{dt}{dx} \tag{35}$$

Rearrange Eq. (30), Eqs. (17) and (18) to obtain the compatibility equation as results

$$\begin{bmatrix} 1 & 0 & 0 & \frac{1}{g} \\ 0 & \frac{g}{a^2} & 1 & 0 \\ dx & dt & 0 & 0 \\ 0 & 0 & dx & dt \end{bmatrix} \begin{bmatrix} H_x \\ H_t \\ V_x \\ V_t \end{bmatrix} = \begin{bmatrix} -\frac{f}{2Dg}V|V| \\ 0 \\ dH \\ dV \end{bmatrix} \tag{36}$$

but this equation is equivalent to Eq. (3-17) through little manipulation so that it follows the same procedure to get the compatibility equations as a method based on Cramer's rule.

2.5 FINITE DIFFERENCE EQUATIONS

So far the different methods are reviewed and the two PDEs of continuity and momentum conservations are transformed into four ODEs that is solved numerically using finite difference techniques. The method of characteristics transformation of the unsteady pipe flow equations gives the water hammer compatibility equations which are valid along the characteristic lines[1,2]:

- along the C+ characteristic line ($\Delta x/\Delta t$ = a):

$$H_{i,t} - H_{i-1,t-\Delta t} + \frac{a}{gA}(Q_{i,t} - Q_{i-1,t-\Delta t}) + \frac{f\Delta x}{2gDA^2}Q_{i,t}|Q_{i-1,t-\Delta t}| = 0 \tag{37}$$

- along the C- characteristic line ($\Delta x/\Delta t$ = -a):

$$H_{i,t} - H_{i+1,t-\Delta t} - \frac{a}{gA}(Q_{i,t} - Q_{i+1,t-\Delta t}) - \frac{f\Delta x}{2gDA^2}Q_{i,t}|Q_{i+1,t-\Delta t}| = 0 \tag{38}$$

in which H = piezometric head, Q = flow rate, Δx = reach length, t = time, Δt = time step, a = water hammer wave speed, g = gravitational acceleration, f = Darcy-Weisbach friction factor, D = pipe diameter and i = node number. At a boundary(reservoir, valve), the boundary equation replaces one of the water hammer compatibility equations. The staggered grid is used in this work[1,9].

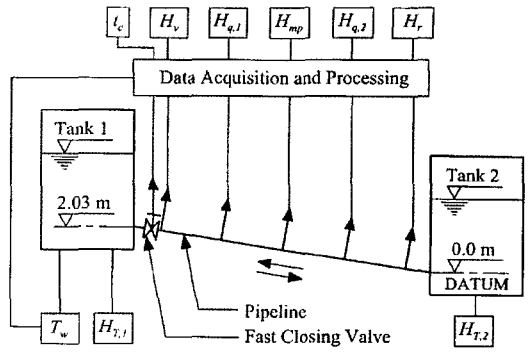

Fig. 2 Experimental apparatus layout[9]

3. FLUID TRANSIENT ANALYSIS

3.1 MODEL VALIDATION

The model validation is conducted through a comparison with results of the standard water hammer algorithms and experimental data[9]. A flexible laboratory apparatus for investigating water hammer and column separation events in pipelines has been designed and constructed. The apparatus is comprised of a straight 37.23 m long sloping copper pipe of 22.1 mm internal diameter and 1.63 mm wall thickness connecting two pressurized tanks and data acquisition and processing as shown in Fig. 2. The pipe slope is constant at 5.45 %.

Water hammer events in the apparatus are initiated by fast closing ball valve positioned at the downstream end of the upward sloping pipe. Fast closure of the valve is carried out either by a torsional spring actuator (the closure time (tc) may be set from 5 to 10 milliseconds) or manually by hand. The flow conditions, identical for the three runs, were:

- static head in an upstream tank $H_{T,2}$ = 32. m
- valve closure time t_c = 0.009 s
- water hammer wave speed a = 1319 m/s

Computational and experimental results for the three runs are compared at the valve and at the midpoint. The experimental run with flow velocity V_0= 0.20 m/s

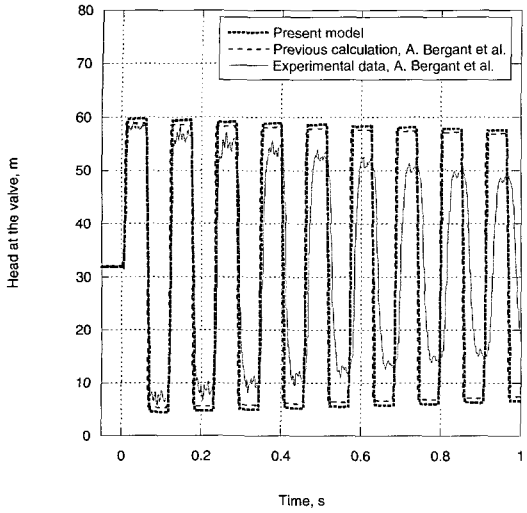

Fig. 3 Comparison of heads at the valve in upward slopping pipe; $V_0 = 0.02$ m/s

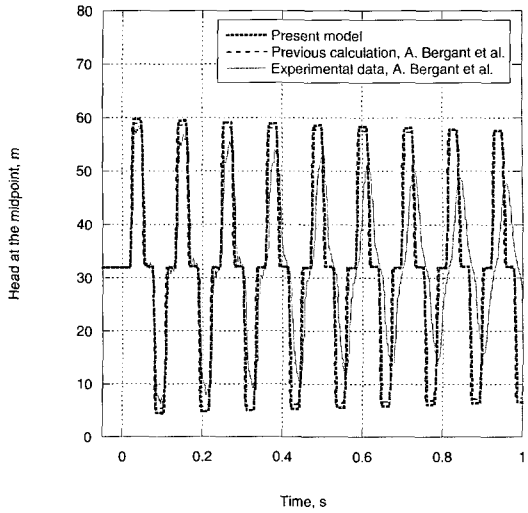

Fig. 4 Comparison of heads at the midpoint in upward slopping pipe; $V_0 = 0.02$ m/s

is the turbulent flow case with Reynolds number Re = 3750(water temperature T_w = 15.4 ℃). Computational results from the present model and the previous model are compared with results of measurements and are depicted in Figs. 3 and 4. Computational results obtained by the quasi-steady friction model agree well for the first period of the transient(4L/a). The discrepancies between the results are apparently magnified for later times. It is usually known that the experimental validation of steady friction models for rapid transients has shown significant discrepancies in attenuation and phase shift of pressure traces when the computational results are compared to the results of measurements[1,8].

The discrepancies are introduced by a difference in velocity profile, turbulence and the transition from laminar to turbulent flow, called the frequency-dependent friction(or unsteady friction) effects. Fortunately, the standard water hammer model is normally sufficiently accurate during early time in a transient. The frequency-dependent influence is most pronounced at high frequencies and in highly viscous flows, and is less significant at high Reynolds numbers[1]. And also a constant value of the Darcy-Weisbach friction factor f (steady state friction factor) is used in most of commercial software packages for water hammer analysis. The unsteady friction effects are not considered in this work.

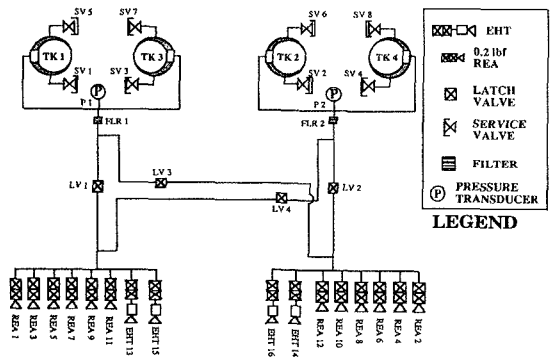

Fig. 5 Schematic of propulsion system

3.2 PROPULSION SYSTEM OF KOREASAT 1

It shows schematic of propulsion system of Koreasat 1 in Fig. 5. It is a hydrazine monopropellant blowdown subsystem. It is divided two independent half-systems each capable of performing all thrusting maneuvers and each half-system consists of two 0.5 m diameter tanks supplying fuel for six 0.9 N catalytic rocket engine assemblies(REAs) and two 0.4 N electrothermal hydrazine thrusters(EHTs). A Ti all-welded manifold network include latching valves, fill and drain valves, filters, pressure and temperature instrumentation, and thermal control equipment. Each half-system will have a normally-open latch valve(LV1 and LV2) which can be closed in the event of leak to

Table. 1 Operation and allowable inlet pressure ranges

Thruster	Operation inlet pressure range (psia)	Allowable inlet pressure range (psia)
REA	400 - 80	420 - 70
EHT	350 - 85	350 - 80

Table. 2 Specific Impulse Requirements

Feed Pressure Range (psia)	Duty Cycle (s)		Isp (minimum)
	On	Off	
350 - 300	0.25	0.75	192
350 - 300	3.00	9.00	216
350 - 100	All others		113
350 - 100	1.0	83.2	137

Table. 3 Case Studies

Pressure (psia)	Thruster valve opening/closing time (ms)		
400	20	10	1
80	20	10	1

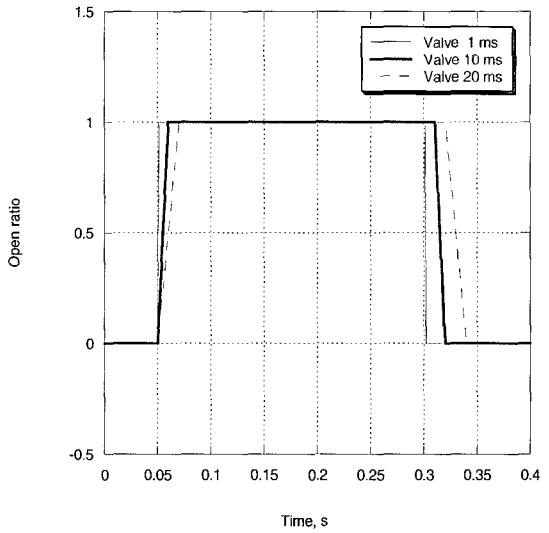

Fig. 6 Thruster Valve Opening/Closing Operations

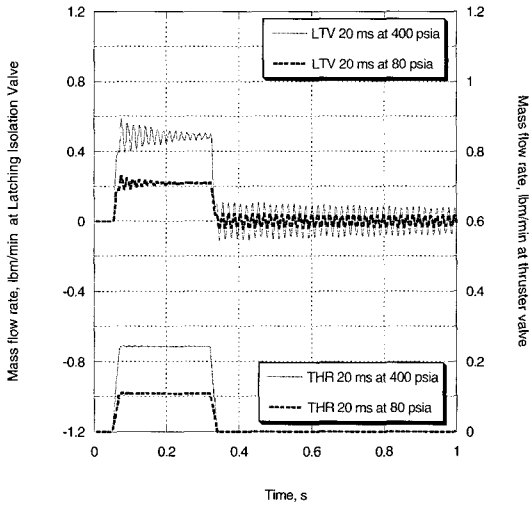

Fig. 7 Mass flow rate of 20 ms w/o orifice

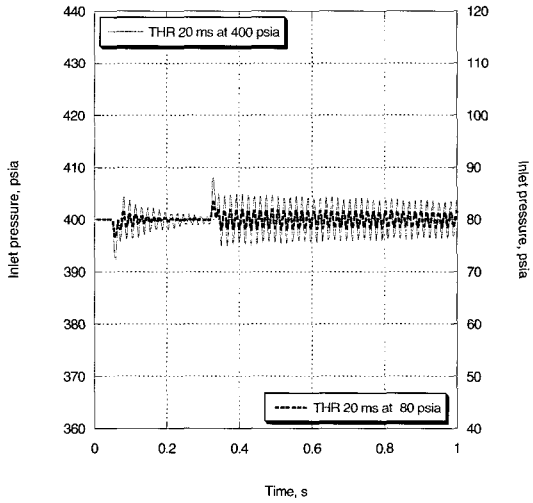

Fig. 8 Inlet Pressure of 20 ms w/o orifice

isolate the tanks of half-system from its thrusters. The cross-over lines are normally closed off by the latching valves(LV3 and LV4), which can be opened if one thruster set must be isolated due to leakage[5].

3.3 THRUSTER VALVE OPERATIONS

The thruster inlet pressure range of the REAs is from 400 psia to 80 psia and EHTs, 350 psia to 85 psia as shown in the Table. 1. The response times of thruster valve are usually less than 20 ms, in this work 1 ms, 10 ms and 20 ms are considered as parameters shown in the Table. 2. Other conditions are the pipeline materials, Ti-3Al-2.5V and 304L SS, an on/off duty cycle of 250 ms on/750 ms off.

In the Table. 2 the specific impulse requirements is shown.

Parametric studies are conducted according to the Table. 3. In Fig. 6 the thruster valve opening/closing times are shown with 250 ms On/750 ms Off.

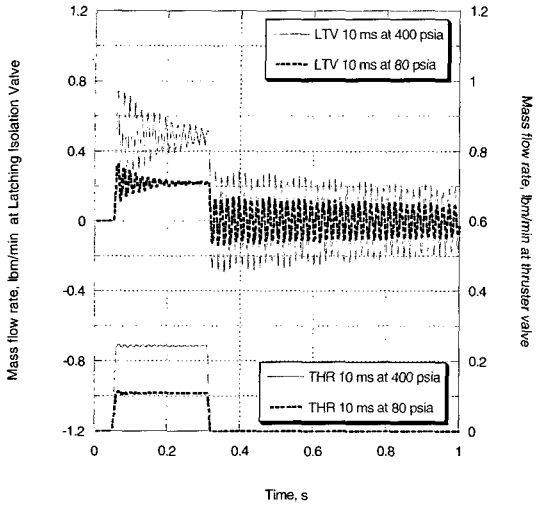

Fig. 9 Mass flow rate of 10 ms w/o orifice

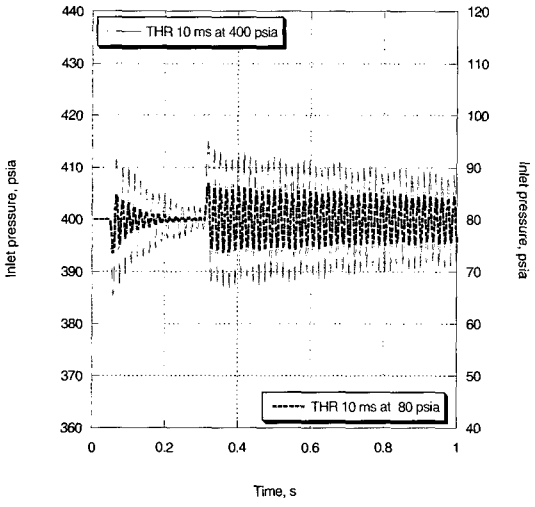

Fig. 10 Inlet Pressure of 10 ms w/o orifice

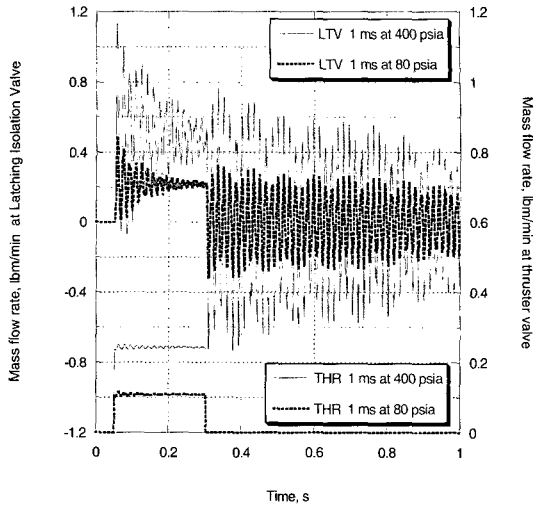

Fig. 11 Mass flow rate of 1 ms w/o orifice

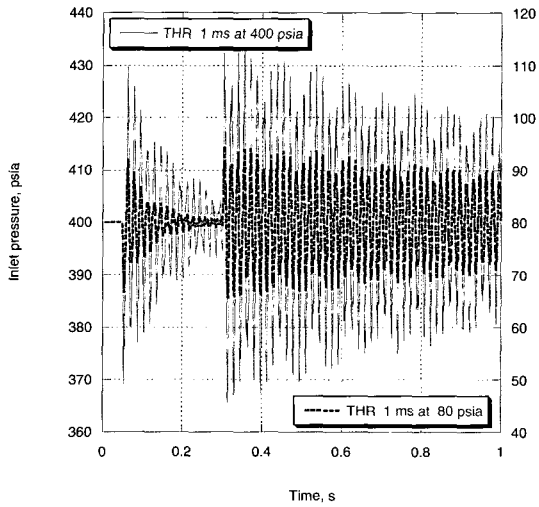

Fig. 12 Inlet Pressure of 10 ms w/o orifice

3.4 RESULTS

The calculations are conducted for the opening and closing thruster valves of REA 5, 6, 7, and 8(Station aquisition: East) at the operation inlet pressure ranges of 400 psia and 80 psia without/with a orifice. Koreast 1 has no orifice, but for a comparison study two orifices(0.048 inch inner-diameter orifice) are selected and installed at the just behind of the filters, FLR1 and FLR2. But this section shows only the results of REA 8 because of similarities of the results.

3.4.1 INLET PRESSURE AT 400 PSIA & 80 PSIA WITHOUT ORIFICE

Because of thruster valve opening/closing the fluid flow rate at the latching isolation valve, LV2 oscillates and the inlet pressure of thruster valve oscillates as shown Figs. 7 and 8, respectively. When the valve is on opening the oscillations of flow rate and pressure attenuate and they go to an steady state. As the valve is on closing the flow rate and pressure oscillate but attenuate at very slow rate. Because there is no flow

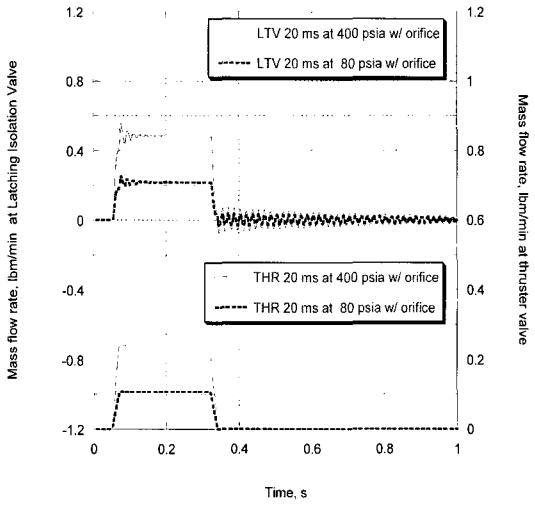

Fig. 13 Mass flow rate of 20 ms with orifice

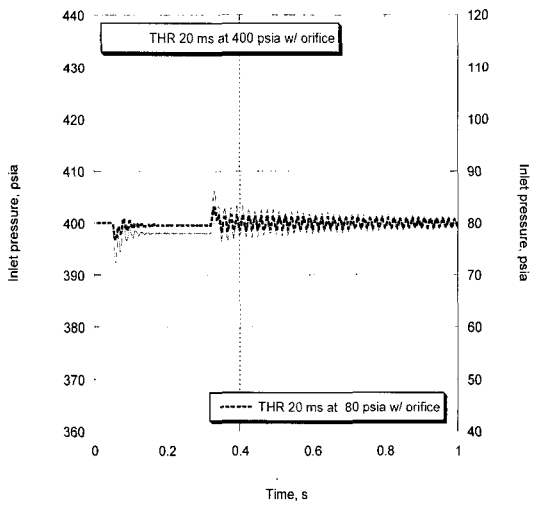

Fig. 14 Inlet Pressure of 20 ms with orifice

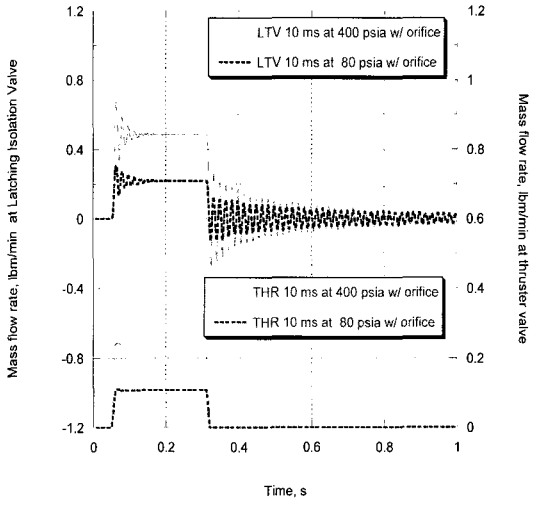

Fig. 15 Mass flow rate of 20 ms with orifice

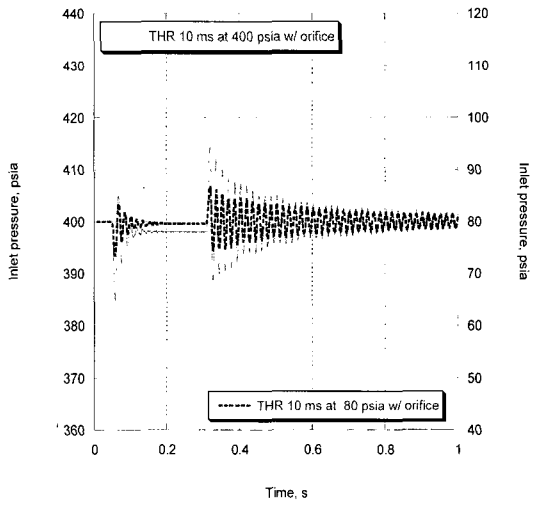

Fig. 16 Inlet Pressure of 20 ms with orifice

control device except the pipeline itself by which friction effect is occurred.

As the inlet pressure of thruster valve is reduced to 80 psia the fluctuations of the fluid flow rate and the inlet pressure of thruster valve are decreased half to the results of 400 psia as shown in Figs. 7 and 8, respectively. This pattern occurs in the results of the other cases.

Because thruster valve opening/closing time is getting shorter, 10 ms, the oscillation amplitudes of fluid flow rate and the inlet pressure of thruster valve are increased as shown Figs. 9 and 10, respectively. When the valve is on opening the oscillations of flow rate and pressure attenuate at relatively fast rate but they do not go to an steady state. The inlet pressure fluctuation of 400 psia case is more than 20 psid so it may have negative effects on the thruster performance.

In worst case the thruster valve opening/closing time is 1 ms, the oscillation amplitudes of fluid flow rate and the inlet pressure are so increased as shown in

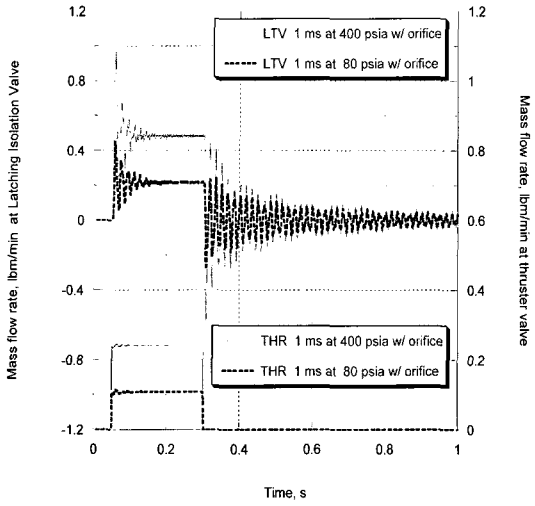

Fig. 17 Mass flow rate of 20 ms with orifice

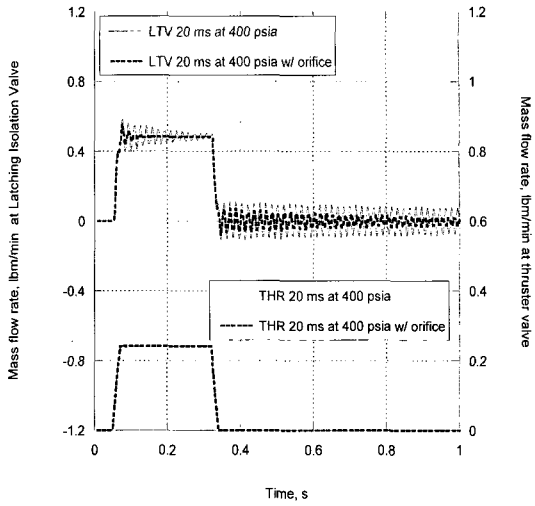

Fig. 19 Mass flow rate of 20 ms at 400 psia w/o and w/ orifice

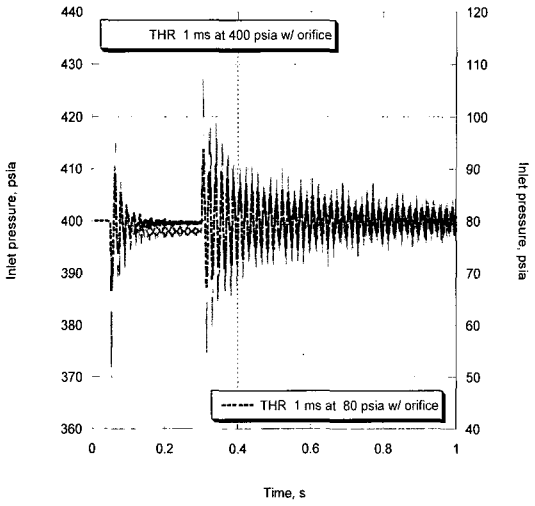

Fig. 18 Inlet Pressure of 20 ms with orifice

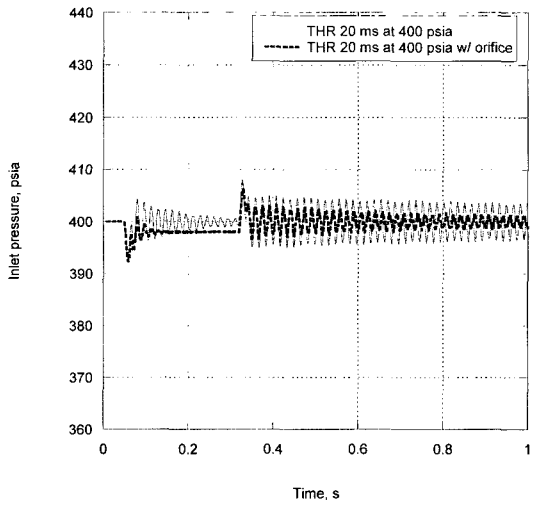

Fig. 20 Inlet Pressure of 20 ms at 400 psia w/o and w/ orifice

Figs. 11 and 12, respectively, that the inlet pressure exceeds the allowable limit in Table 1. The inlet pressure fluctuation of 400 psia case is of more than 60 psid, unless an proper orifice being installed, it may not run at this condition. According to the results as shown in Figs. 18, the 0.048 inch inner-diameter orifice adapted cannot limit the pressure oscillation so that the smaller inner-diameter orifice should be used.

3.4.2 INLET PRESSURE AT 400 PSIA & 80 PSIA WITH ORIFICE

The orifice is selected by referring to the propulsion systems of KOMPSAT program and EO-1(Earth Observing 1) mission. Those propulsion systems are a monopropellant hydrazine system in blow-down mode with maximum expected operating pressure(MEOP) 350 psia and 320 psia, respectively[6,7].

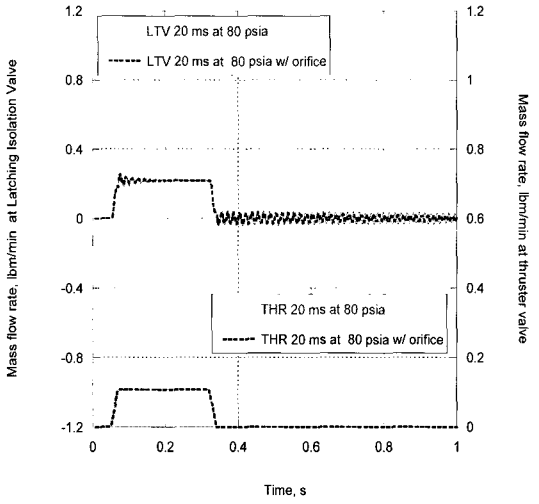

Fig. 21 Mass flow rate of 20 ms at 80 psia w/o and w/ orifice

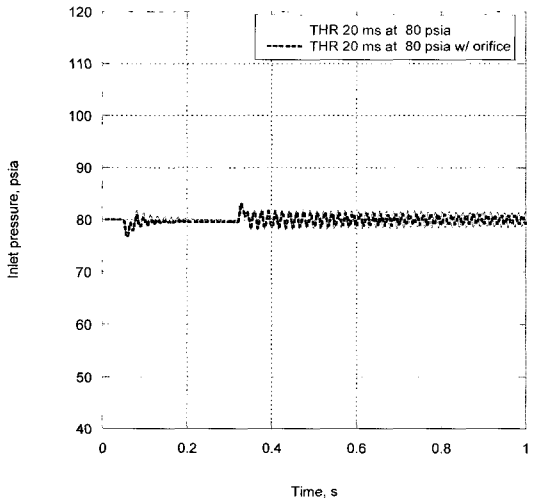

Fig. 22 Inlet Pressure of 20 ms at 80 psia w/o and w/ orifice

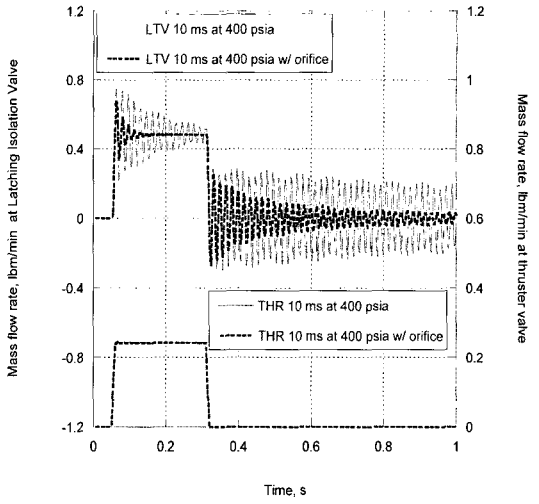

Fig. 23 Mass flow rate of 10 ms at 400 psia w/o and w/ orifice

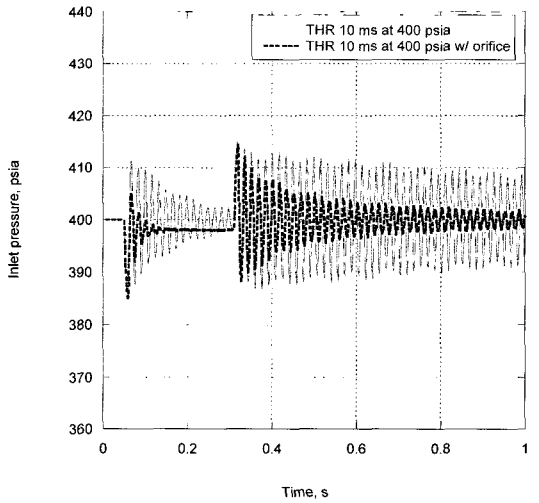

Fig. 24 Inlet Pressure of 10 ms at 400 psia w/o and w/ orifice

As shown in Fig. 13 and 14 when the valve is on opening the oscillations of flow rate and pressure attenuate at apparently fast rate and they go to an steady state rapidly. As the valve is on closing the flow rate and pressure oscillate less than that of without-orifice-case and attenuate at fast rate. Because the orifice limits flow transients. It is hard to find a wiggling of flow rate of the thruster valve in both 400 psia and 80 psia cases.

As the inlet pressure of thruster valve is reduced to 80 psia the fluctuations of the fluid flow rate and the inlet pressure of thruster valve are almost similar to the results of 400 psia without orifice. It seems the effect of orifice is reduced at low inlet pressure.

Due to using the orifice, the oscillation amplitudes of fluid flow rate and the inlet pressure of thruster

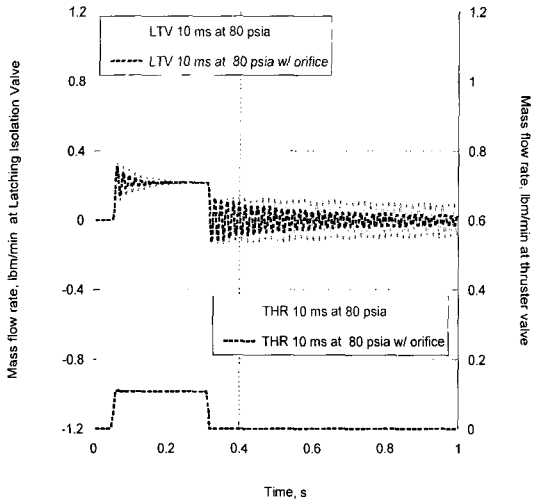

Fig. 25 Mass flow rate of 10 ms at 80 psia w/o and w/ orifice

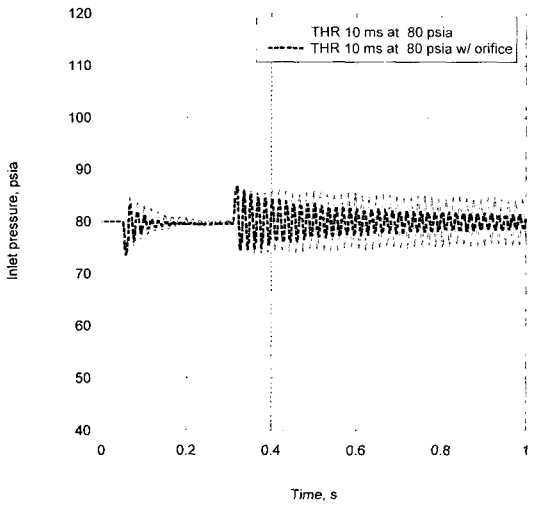

Fig. 26 Inlet Pressure of 10 ms at 80 psia w/o and w/ orifice

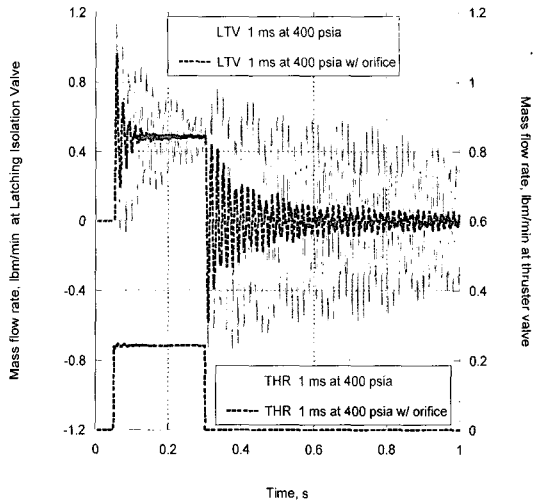

Fig. 27 Mass flow rate of 1 ms at 400 psia w/o and w/ orifice

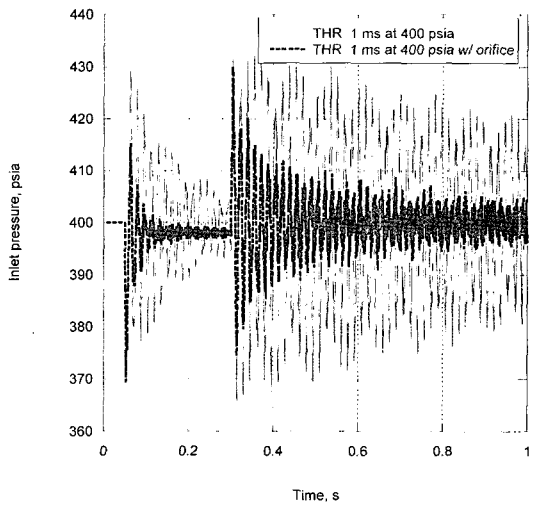

Fig. 28 Inlet Pressure of 1 ms at 400 psia w/o and w/ orifice

valve attenuate rapidly as shown Figs. 15 and 16, respectively.

In worst case the thruster valve opening/closing time is 1 ms, the oscillation amplitudes of fluid flow rate and the inlet pressure attenuate rapidly as shown in Figs. 17 and 18, respectively but inlet pressure oscillation is still so high that it exceeds the allowable operation limit in Table 1.

3.4.3 COMPARISON THE RESULTS BETWEEN WITHOUT-ORIFICE AND WITH-ORIFICE CASES

In this section all the results are presented again in without-orifice and with-orifice cases as shown in Figs. 19 through 30. As it mentioned above, the effect of orifice is so strong to limit the fluid transients in rapid valve response time and at high pressure. But it seems that the effect of orifice weakens at loose valve

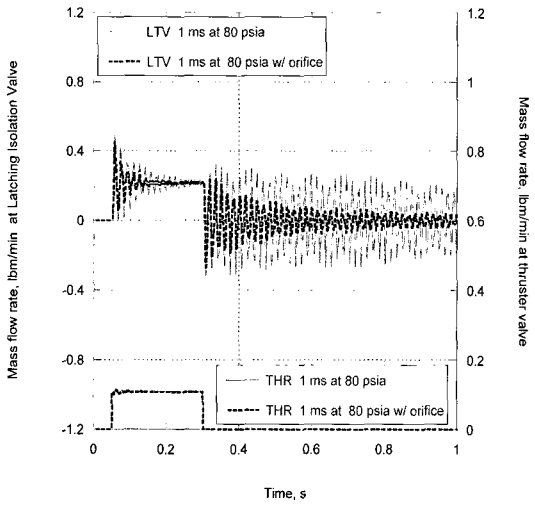

Fig. 29 Mass flow rate of 1 ms at 80 psia w/o and w/ orifice

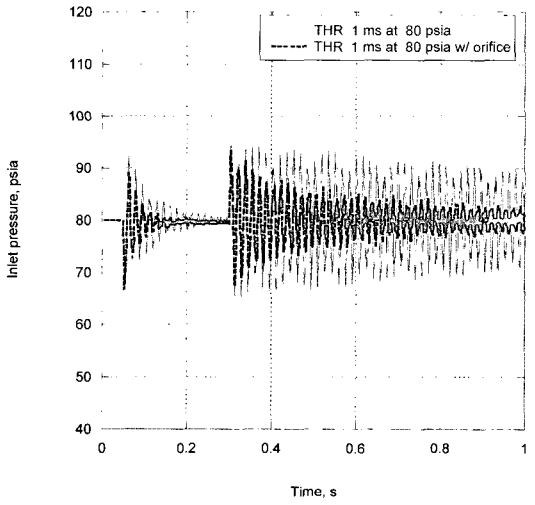

Fig. 30 Inlet Pressure of 20 ms at 80 psia w/o and w/ orifice

response time and at low pressures. Because as the inlet pressure gets down, the line pressure drop due to orifice gets decreased and also flow rate reduced as shown in Figs. 19 through 30.

4. CONCLUSION

This work is to review the different derivation methods that result in the same compatible and characteristic equations in order to understand the method of characteristics extensively.

The identification of fluid transient phenomena of Koreasat 1 is carried out through parametric studies. The valve response time is one of the dominant parameters governing the fluid transient phenomena. The results show that the shorter closing time induces the greater pressure response amplitude.

According to the results it shows that the installation of in-line orifice is effectively to limit the fluid transients in rapid valve response time and at high pressure. But it seems that the effect of orifice weakens at slow valve response time and at low pressures.

ACKNOWLEDGEMENT

The author gratefully acknowledges the financial support of the Ministry of Science and Technology of Korea and appreciates Dr. Anton Bergant who provides his computational and experimental data willingly.

REFERENCES

[1] Wylie, E.B. et al., 1993, *Fluid Transients in Systems*, Prentice Hall, Upper Saddle River, pp.37-42.

[2] Thorley, A.R.D., 2004, *Fluid Transients in Pipeline Systems*, ASME Press, pp.102-114.

[3] Walski, T.M. et al., *Advanced Water Distribution Modeling & Management*, http://www.haestad.com.

[4] Anderson, Jr., J.D., 1995, *Computational Fluid Dynamics*, McGraw-Hill, New York, pp.97-105.

[5] ---, KOREASAT 1 CDR Propulsion Subsystem, 1993, *GE Aerospace Astro-Space Division*, Princeton.

[6] Choi, H.S., 1999, "KOMPSAT-1 Propulsion Subsystem Fluids Analysis," *TM, KARI.*

[7] *Earth Observing 1 Satellite*, NASA, http://eo1.gsfc.nasa.gov/.

[8] BERGANT A., et al. 2001, "Developments in unsteady pipe flowfriction modelling", *JOURNAL OF HYDRAULIC RESEARCH*, VOL.39, NO.3, pp.249-257.